Since January 2020 Elsevier has created a COVID-19 resource centre with free information in English and Mandarin on the novel coronavirus COVID-19. The COVID-19 resource centre is hosted on Elsevier Connect, the company's public news and information website.

Journal of Colloid and Interface Science 606 (2022) 961–970

Contents lists available at ScienceDirect

Journal of Colloid and Interface Science

journal homepage: www.elsevier.com/locate/jcis

Biodegradable and high-performance multiscale structured nanofiber membrane as mask filter media via poly(lactic acid) electrospinning

Ling Wang, Yanfei Gao *, Junpeng Xiong, Weili Shao *, Chen Cui, Ning Sun, Yuting Zhang, Shuzhen Chang, Pengju Han, Fan Liu, Jianxin He

Textile and Garment Industry of Research Institute, Zhongyuan University of Technology, Zhengzhou 450007, People's Republic of China
International Joint Laboratory of New Textile Materials and Textiles of Henan Province, Zhengzhou 450007, People's Republic of China

HIGHLIGHTS

- A true-nanoscale PLA nanofiber with an average size of 37 ± 4 nm was fabricated.
- The multi-scale structured nanofiber membrane was designed by one-step method, and the performance parameters were optimized.
- The mask filter made of multi-scale structured nanofiber membrane showed high filtration efficiency and breathability.
- The resultant mask filter has biodegradability and would be a great substitute for existing commercial masks in the future.

GRAPHICAL ABSTRACT

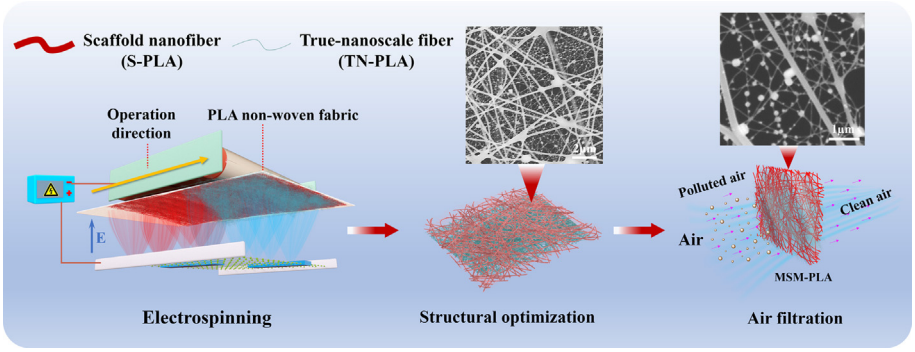

ARTICLE INFO

Article history:
Received 13 July 2021
Revised 11 August 2021
Accepted 12 August 2021
Available online 17 August 2021

Keywords:
Electrospinning
Poly(lactic acid)
Multiscale structure
Air filtration
Biodegradability

ABSTRACT

The usage of single-use face masks (SFMs) has increased since the outbreak of the coronavirus pandemic. However, non-degradability and mismanagement of SFMs have raised serious environmental concerns. Moreover, both melt-blown and nanofiber-based mask filters inevitably suffer from poor filtration performance, like a continuous decrease in the removal efficiency for particulate matter (PM) and weak breathability. Herein, we report a new method to create biodegradable and reusable fibrous mask filters. The filter consists of a true nanoscale bio-based poly(lactic acid) (PLA) fiber (an average size of 37 ± 4 nm) that is fabricated via electrospinning of an extremely dilute solution. Furthermore, we designed a multi-scale structure with integrated features, such as low basis weight (0.91 g m^{-2}), small pore size (0.73 μm), and high porosity (91.72%), formed by electrospinning deposition of true nanoscale fibers on large pore of 3D scaffold nanofiber membranes. The resultant mask filter exhibited a high filtration efficiency ($PM_{0.3}$–99.996%) and low pressure drop (104 Pa) superior to the commercial N95 filter. Importantly, this filter has a durable filtering efficiency for PM and natural biodegradability based on PLA. Therefore, this study offers an innovative strategy for the preparation of PLA nanofibers and provides a new design for high-performance nanofiber filters.

1. Introduction

The ongoing coronavirus disease (COVID-19) pandemic has led to an increase in the usage of nonwoven single-use face masks

* Corresponding author at: Textile and Garment Industry of Research Institute, Zhongyuan University of Technology, Zhengzhou 450007, People's Republic of China.
E-mail addresses: 807008820@qq.com (Y. Gao), weilishao@163.com (W. Shao).

https://doi.org/10.1016/j.jcis.2021.08.079
0021-9797/

(SFMs), with monthly estimated use of 129 billion face masks globally [1-4]. However, the extensive use and improper disposal of face masks further aggravate plastic pollution on coasts and beaches [5,6]. A report released by the marine conservation organization, OceansAsia, had suggested that an estimated 1.56 billion face masks entered marine environment in 2020 alone [7]. These masks could take 450 years to completely decompose, slowly converting to microplastics while negatively affecting marine wildlife and might even entering human food chains [8–10].

A major contributor to this problem is the commonly used SFM, which comprises undegradable petro-based polypropylene (PP) melt-blown filter media [11]. This type of filter media can effectively capture ultrafine particles through electrostatic adsorption because it is charged after electret treatment. However, the removal efficiency of SFMs decreases continuously because of the weakening of electrostatic adsorption associated with charge dissipation in moist human breath [12–14]. In addition, a short service life and frequent mask changes, which further aggravates the waste of environmental resources [15].

In contrast, nanofiber-based filter media has a reduced diameter, high specific surface area, and high porosity [16–18]. Moreover, it exhibits improved durability of filtration mainly through physical sieving, making it a promising candidate for air purification [19–22]. In the early stage of this work [23], nanofiber electret anti-haze window screens were fabricated by doping Si_3N_4 into the PU nanofibers. They exhibited a removal efficiency of 79.36% and a pressure drop of 25 Pa. However, despite improved filtration performance, conventional nanofiber filters still require a high thickness to improve further the removal efficiency for $PM_{0.3}$ (particulate matters (PMs) with the most-penetration size of 300 nm). Due to their pseudo-nanoscale diameter (usually > 100 nm), the air resistance is compromised, leading to rough breathing when the filters are used in masks or respirators [24–26]. Therefore, there is growing interest in developing nanofiber filters with integrated filtration performance by further reducing the fiber diameter below 100 nm. Zhang et al. [27] created a poly(m-phenylene isophthalamide) nanofiber/net air filter with a bimodal structure composed of scaffold nanofibers and 2D nanonets with true nanoscale diameters (~20 nm) via electrospinning/netting. The composite membranes were capable of impeding the penetration of 300–500 nm particles with a high removal efficiency of 99.999% and low pressure drop of 92 Pa. Zuo et al. [28] prepared free-standing polyurethane (PU) nanofiber/net air filters, including bonded nanofibers and 2D nanonets, with a diameter of ~ 20 nm by integrating an electrospinning/netting technique and a facile peel-off process from the designed substrates. The resultant filters possessed > 99.97% filtration efficiency with ~ 40% transmittance for $PM_{0.3}$ filtration and purification capacity for real smoke $PM_{2.5}$ filtration. In addition, Liu et al. [29] used a humidity-induced electrospinning technology to fabricate polyacrylonitrile nanofiber/nets with dual-network structures containing 2D ultrafine (~20 nm) nanonets bonded with nanofiber scaffolds, which exhibited high porosity (93.9%), high $PM_{0.3}$ removal efficiency (>99.99%), low air resistance (only < 0.11% of atmospheric pressure), and promising purification of $PM_{2.5}$. However, the application of biodegradable true nanoscale fibers in air filter materials, such as masks and respirators, has rarely been reported [30–32]. Moreover, the preparation of environment-friendly bio-based and biodegradable poly(lactic acid) (PLA) nanofibers < 50 nm has not been reported yet [33,34].

Herein, we report a method to prepare a biodegradable, reusable, durable, breathable, and highly efficient face mask filter with a multiscale structure based on green biodegradable PLA. The feature of our design is that the true-nanoscale PLA fibers (TN-PLA) were successfully fabricated for the first time via electrospinning technology. Further, we designed a multiscale structure formed by electrospinning deposition of TN-PLA on the large pores of 3D scaffold nanofiber membranes (S-PLA). The multiscale structure was optimized by tailoring the fiber density ratio of TN-PLA to S-PLA, which possessed integrated features, such as small pore size, high porosity, and narrow pore size distribution. The resultant face mask filters exhibited comprehensive performance, including robust $PM_{0.3}$ removal capacity and low air resistance. More significantly, this filter has a durable recycling performance in filtration PM and biodegradability.

2. Experimental part

2.1. Materials

PLA (Mr = 200000) was purchased from NatureWorks, Co., Ltd., USA. Tetrabutylammonium chloride (TBAC, $C_{16}H_{36}ClN$) was supplied by Jiangsu Baoze Polymer Materials Co., Ltd., China. N, *N*-dimethylformamide (DMF) (≥99.0%), Dimethyl carbonate (DMC) (≥99.0%), alcohol (≥99.0%), and sodium chloride (NaCl) were obtained from Xilong Scientific Co., Ltd., China. All the chemicals were analytically pure and used without further purification. Mosquito killing tablets were purchased from Jingzhou Yangchang Daily Chemical Co., Ltd., China. PLA nonwoven fabric (20 g m^{-2}) was kindly supplied by Jiangxi Haorui Industrial Materials Co., Ltd., China. Commercial 3 M respirator were purchased from Minnesota Mining and Manufacturing Co. (3 M Co.), USA.

2.2. Preparation of PLA solutions

Precursor solutions were prepared using PLA, TBAC, DMC, and DMF. To fabricate scaffold nanofibers, 0.5 wt% TBAC was dissolved in DMC/ DMF (7/3) solvent and stirred for 3 h at 50 °C. Subsequently, PLA was added to the TBAC solution at concentrations of 9, 11, 13, and 15 wt% of the solution mass and stirred for 5 h at 70 °C. These solutions are denoted as PLA-0.5 T solutions. Similarly, another type of solution was prepared using PLA, TBAC, and DMC/ DMF (5/5); the concentrations of PLA were 3, 5, 7, and 9 wt%, respectively, whereas the TBAC was kept constant at 7 wt% to significantly enhance the conductivity of the solutions. The resulting solutions are denoted as PLA-7 T solutions.

2.3. Fabrication of PLA fibrous membranes

The electrospinning process was conducted using a modular electrospinning machine (Zhongxian New Material Co., China). The prepared PLA-0.5 T solutions were loaded into six spinning units and pumped out at a speed of 10 mm min^{-1}. The PLA nanofiber membranes were prepared under a constant voltage of 25 kV and a spinning distance of 18 cm. Subsequently, the resultant nanofibers were deposited on the nonwoven substrate that covered the stainless receiver at a receiving speed of 0.08 m min^{-1}. Similarly, PLA nanofiber membranes were fabricated using the PLA-7 T precursor solution at a spinning voltage of 25 kV, 18 cm distance, and 5 mm min^{-1} feed rate. According to the following morphology characterization, PLA-0.5 T with 11 wt% and PLA-7 T with 3 wt% concentrations were selected to fabricate S-PLA and TN-PLA, respectively. Subsequently, the fabricated S-PLA and TN-PLA solutions were loaded into a certain number of spinning units. The total number of spinning units was six. By tailoring the number of S-PLA and TN-PLA spinning units, various multiscale structured PLA nanofiber membranes with different spinning unit ratios (0/6, 1/5, 2/4, 3/3, 4/2, 5/1, TN-PLA/S-PLA) were prepared at the same receiving speed (0.08 m min^{-1}). Membranes with different weights were designed by varying the receiving speed. The receiving speed was 0.04–0.2 m min^{-1}. The spinning experiment

was conducted at a constant temperature of 25 ± 3 °C and humidity of 30 ± 3%.

2.4. Nanofiber membrane characterization

The viscosity and conductivity of the solution were measured using a digital viscometer (RVAV-1, Shanghai Yueping Scientific Instrument Co., Ltd., China) and a conductivity meter (DDS-307, Hangzhou Qiwei Instrument Co., Ltd., China). Scanning electron microscopy (SEM, PW-100–515, Shanghai Fona Scientific Instrument Co., Ltd., China) was performed to observe the morphology of the nanofiber membranes. The pore size and porosity of the nanofiber membranes were investigated using a high-performance automatic mercury porosimeter (Autopore IV 9500, Micromeritics). The mechanical properties of the membranes were investigated using an XLW (EC) type tensile strength tester, and their thicknesses were tested using a CH-12.7-STSX digital thickness tester. Hydrophilicity and hydrophobicity were investigated using a contact angle tester (Dataphysics OCA 15EC, Germany).

2.5. Filtration performance test

The filtration performance of composite membranes for rigid solid particles (NaCl) with a mass mean diameter of 300–500 nm was evaluated using a TSI 8130 automated filter material detector under different airflow rates. The $PM_{2.5}$ recycling purification measurement was performed using a self-designed device. Smoke was generated by burning mosquito killing tablets. The PM detectors were provided by Beijing Air Housekeeper Technology Co., Ltd. The filtration efficiency and air resistance of the PM were calculated using the following formulas [35,36]:

$$\eta = \frac{C_{in} - C_{out}}{C_{in}} \times 100\%$$

where C_{in} and C_{out} represent the particle concentrations upstream and downstream of the filter, respectively.

$$\Delta P = P_{in} - P_{out}$$

where ΔP is the pressure drop of the filter.

The quality factor (Q_f) is often used as a representative tool to directly reflect the overall filter performance. The formula is as follows [37,38]:

$$Q_f = \frac{-In(1-\eta)}{\Delta P}$$

2.6. Biodegradation test

Enzymatic degradation of the composite nanofiber membrane was investigated using proteinase K. The degradation process parameters were as follows: original pH of the solution was 9.0, temperature was 60 °C, and proteinase K concentration was 0.4 mg ml^{-1}. The weight of the filter was measured every 2 h. In addition, soil burial degradation under natural conditions was car-

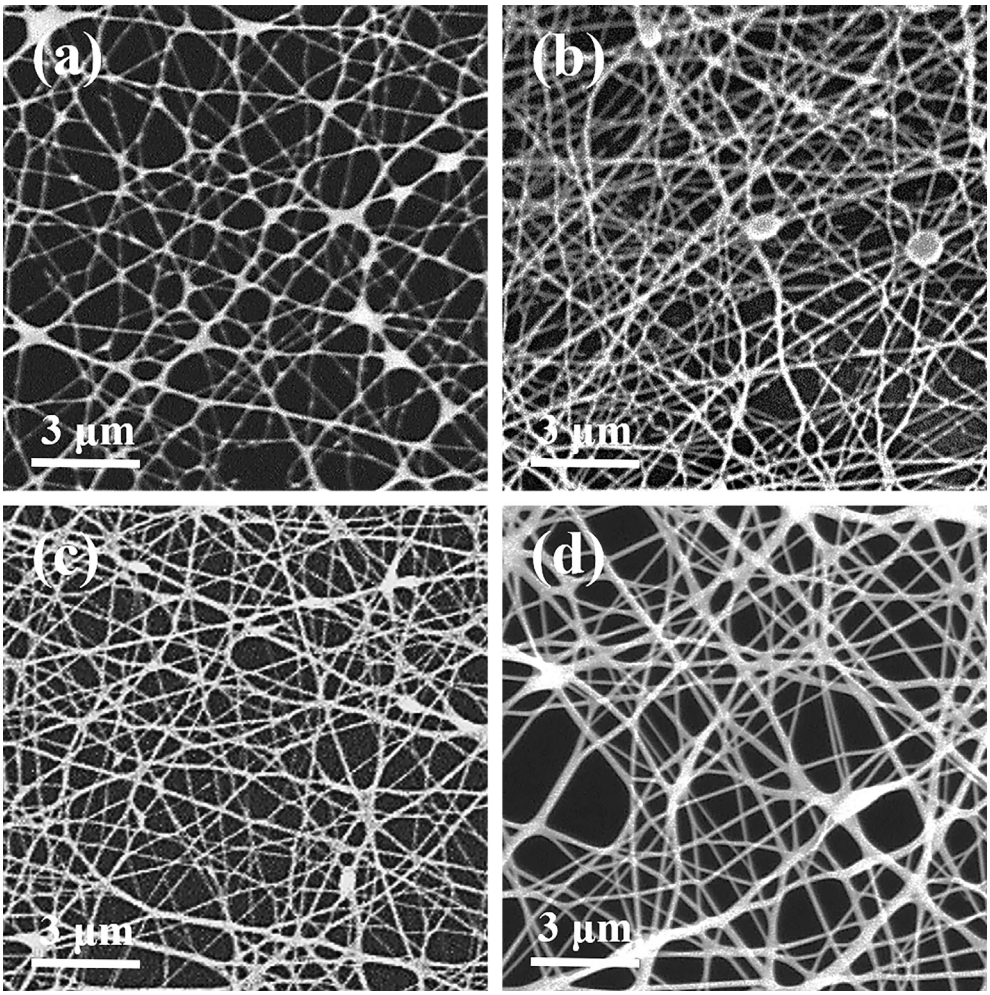

Fig. 1. SEM images of the PLA nanofiber membranes obtained from solutions with PLA concentration of (a) 3, (b) 5, (c) 7 and (d) 9 wt%.

ried out on the Zhongyuan University of Technology campus. The samples were dried in an oven at 50 °C and weighed before burial. Several groups of samples were buried in the soil at a depth of 15 cm for 150 d. Soil temperature, humidity, and pH mainly depend on natural degradation, and the microorganisms in the degradation process originate from the microbial community in natural soil. Weight loss during soil burial degradation was measured every 10 days. The soil was carefully and completely removed using water, dried in an oven at 50 °C until constant weight, and then weighed. The percentage of weight loss (WL) in the degradation of a sample was calculated using the following equation [39–41]:

$$WL = \frac{M_b - M_a}{M_b} \times 100\%$$

where M_b and M_a are the weights of the sample before and after degradation, respectively.

3. Results and discussion

3.1. Design of multiscale structured membranes

First, various coarse nanofibers with different concentrations of PLA were fabricated, and their SEM images and representative diameter distributions are shown in Figs. S1 and S2. The properties, including the viscosity and conductivity of the spinning solution, are shown in Fig. S3. The 11% PLA nanofibers with an average diameter of 187 ± 13 nm had a uniform diameter distribution and no beads, which were used as S-PLA.

Next, the spinning parameters of the ultrafine nanofibers were optimized, and the morphologies and representative diameter distributions of the nanofibers with different PLA concentrations are shown in Figs. 1 and S4. The properties of the spinning solutions and representative diameter distributions are shown in Fig. S5. The average diameter of the 9% PLA nanofibers was the largest (105 ± 13 nm). Further decreasing the concentration to 3% resulted in a significant reduction in the diameter of the uniform fibers to 37 ± 4 nm, and the nanofiber network composed of fine fibers pos-

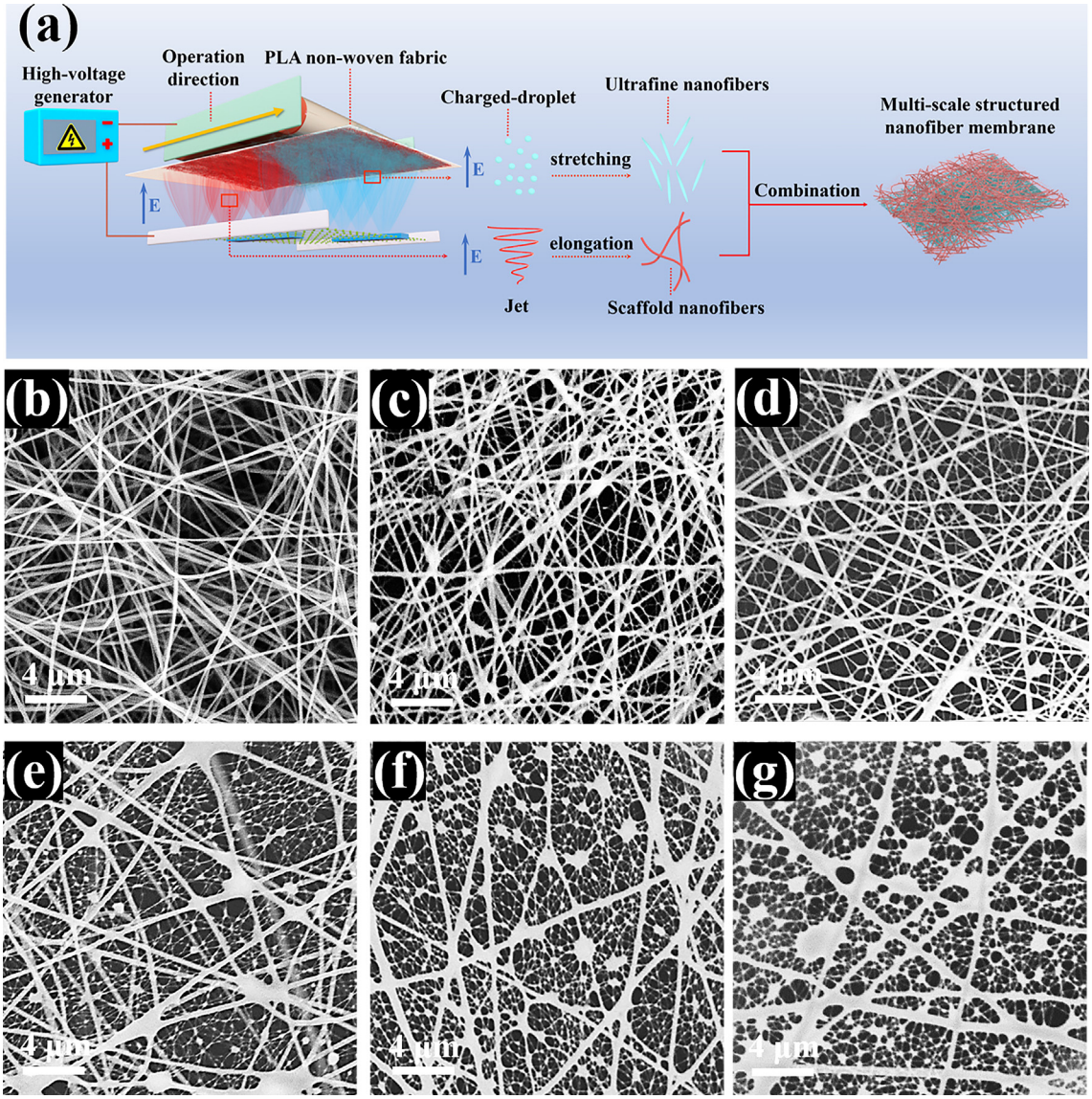

Fig. 2. (a) Schematic diagram showing fabrication process of multi-scale structured nanofiber membranes. SEM images of the multi-scale structured membranes with the number of spinning unit ratio of (b) 0/6, (c) 1/5, (d) 2/4, (e) 3/3, (f) 4/2, (g) 5/1.

sessed a complete structure. This is mainly because under the condition of high conductivity and extremely dilute solution, numerous charged droplets were ejected from the needle in the high-pressure electrostatic field rather than the traditional electrospinning jet mode. These charged droplets are rapidly elongated to ultrafine fibers under the action of an electric field force, and the network structure was constructed by stacking superfine nanofibers. The formation process of the superfine fibers is shown in Fig. 2a. Subsequently, we designed a multiscale structure formed by TN-PLA electrospinning deposition on the large pores of 3D S-PLA.

Various multiscale structured PLA nanofiber membranes (MSM-PLA) were prepared by adjusting the number of spinning unit ratios of TN-PLA to S-PLA (0/6, 1/5, 2/4, 3/3, 4/2, 5/1, 6 spinning units in total). The SEM images of multiscale structured membranes with different ratios are shown in Fig. 2b-f. The average diameter of TN-PLA (37 ± 4 nm) was one order of magnitude lower than that of the S-PLA (187 ± 13 nm). The TN-PLAs divided the pores formed by the S-PLAs into numerous small pores, forming an irregular grid. With an increase in TN-PLA, the network aperture decreased. It is worth noting that when the ratio was 4/2 or 5/1, there are many "small solid films" bonded to the nanofibers. This indicates that a further increase in proportion of spinning units of the TN-PLA would affect the pore structure of the MSM-PLA.

3.2. Multiscale structured membranes characterization

To further demonstrate the impact of the spinning unit ratio on the pore structure, the pore diameter distribution, average pore diameter, and porosity of MSM-PLA with different ratios were investigated systematically, as shown in Fig. 3a-b. These parameters of porous membrane filters have a significant impact on the filtration performance [42,43]. Compared to the pure S-PLA membrane (the ratio of 0/6), MSM-PLA containing TN-PLA showed decreased pore size and narrower distribution; the pore size reduced from 1.83 μm to 1.72 μm, 1.23 μm, 0.73 μm, 0.56 μm, and 0.26 μm. When the ratio of TN-PLA to S-PLA changed from 0/6 to 1/5, 2/4, and 3/3, the porosity of the composite nanofiber membrane increased from 86.2% to 86.93%, 88.64%, and 91.72%, respectively. However, with further increases in the TN-PLA content from 3/3 to 4/2 and 5/1, the porosity decreased from 91.72% to 90.82% and 89.53%, respectively. This may be attributed to the highly dense packing of TN-PLA and the increase of small solid films, which is in good agreement with the morphological characteristics.

The mechanical properties of multiscale structured membranes are the premise to ensure the stability of membrane filtration performance during use. The results are shown in Figs. 3c and S6. The tensile strength and Young's modulus are positively correlated with the content of TN-PLA, which is mainly due to the fewer structural defects of finer fibers, the higher degree of orientation of molecular chains along the fiber axis, and the reduction of stress concentration attributed to the network structure formed by TN-PLA in the pores of the scaffold fibers. The decrease in strain from 3/3 to 4/2 and 5/1 might be attributed to the decrease in the elongation of multiscale structured membranes due to the increase in the solid membrane. Among them, the membranes with a ratio of 3/3 possessed the highest elongation at break (54.13%) and had appropriate mechanical properties (tensile strength of 10.52 MPa, Young's modulus of 173 MPa).

In addition to the above performance, for masks, appropriate hydrophobicity can effectively prevent water vapor adsorption on the filter, which maintains the material with high filtration efficiency and low respiratory resistance [22]. Fig. 3d shows that the

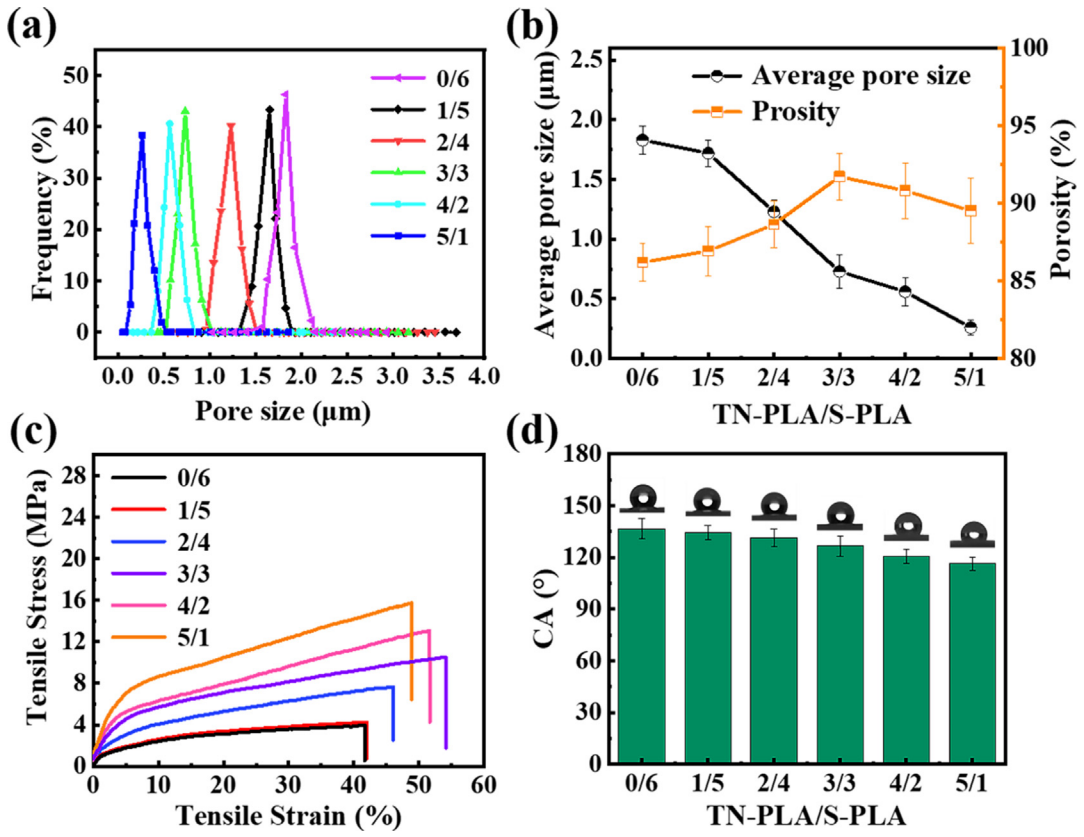

Fig. 3. (a) Pore size distribution, (b) average pore size and porosity, (c) mechanical properties and (d) water contact angle (WCA) of multi-scale structured membranes with various number of spinning unit ratios of TN-PLA to S-PLA.

water contact angle (WCA) of multiscale structured membranes decreased significantly to 116.3°, compared to the WCA of 136.7° for the pure S-PLA membrane (0/6). This might be ascribed to the high content of TBAC (a type of salt with strong hygroscopicity) in TN-PLA and the high specific surface area of TN-PLA. It is noteworthy that the membranes had a proper contact angle of 126.6° when the spinning unit ratio was 3/3. Moreover, the water droplet on the membrane remained spherical for 8 h (Fig. S8), which indicates the stable hydrophobicity of the 3/3 multiscale structured membrane.

3.3. Air filtration performance of MSM-PLA

The filtration performance of various membranes was investigated under an airflow velocity of 32 L/min according to the latest standard (EN779:2012) for air filters. Fig. 4a shows the filtration efficiency and air resistance for the most permeable (~300 nm) rigid solid NaCl particles. Compared with the pure S-PLA membrane with a lower Q_f value (Fig. S7), all MSM-PLA with different ratios exhibited improved filtration efficiency, which indicated that a moderate increase in the proportion of TN-PLA was conducive to enhancing the filtration capacity of the composite membrane. With an increase in the TN-PLA content, the Q_f value of MSM-PLA increased from 0.059 Pa^{-1} to 0.097 Pa^{-1} for NaCl $PM_{0.3}$ (Fig. 4b), mainly because the combination of increased porosity and decreased pore size would help reduce the airflow resistance and improve the particle trapping ability [44] (Fig. 4c). When spinning units ratio was 3/3, the composite membrane had the highest Q_f value of 0.097 Pa^{-1}, with high filtration efficiency of 99.996%, and maintaining low air resistance of 104 Pa. It is noteworthy that

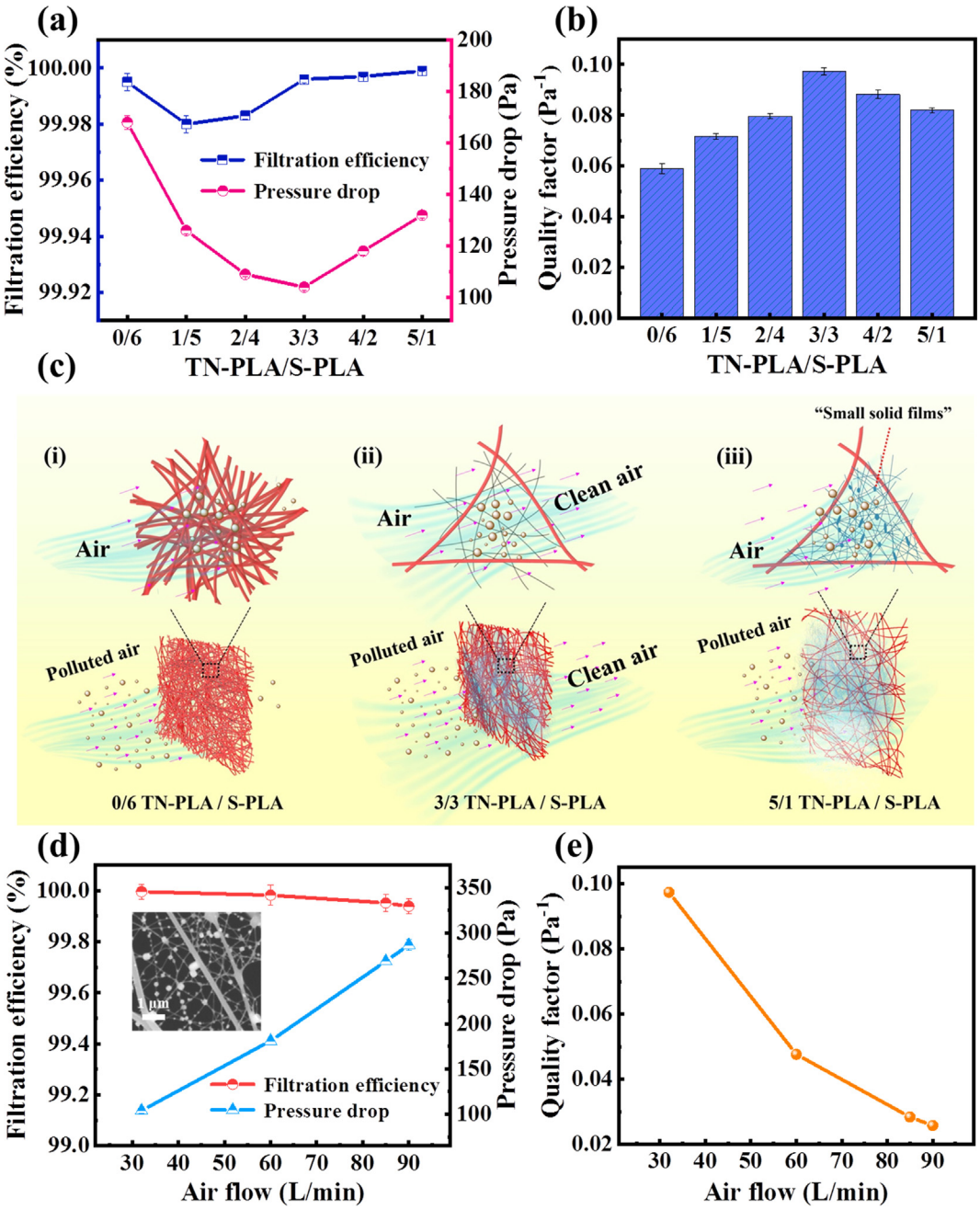

Fig. 4. (a) Filtration performance and (b) quality factor of multi-scale structured membranes with different number of spinning unit ratios of TN-PLA to S-PLA. (c) Schematic diagram of filtration mechanism of MSM-PLA with different ratios of TN-PLA to S-PLA including (i) 0/6, (ii) 3/3, (iii) 5/1. d) Filtration performance and (e) quality factor of the multi-scale structured membranes (3/3).

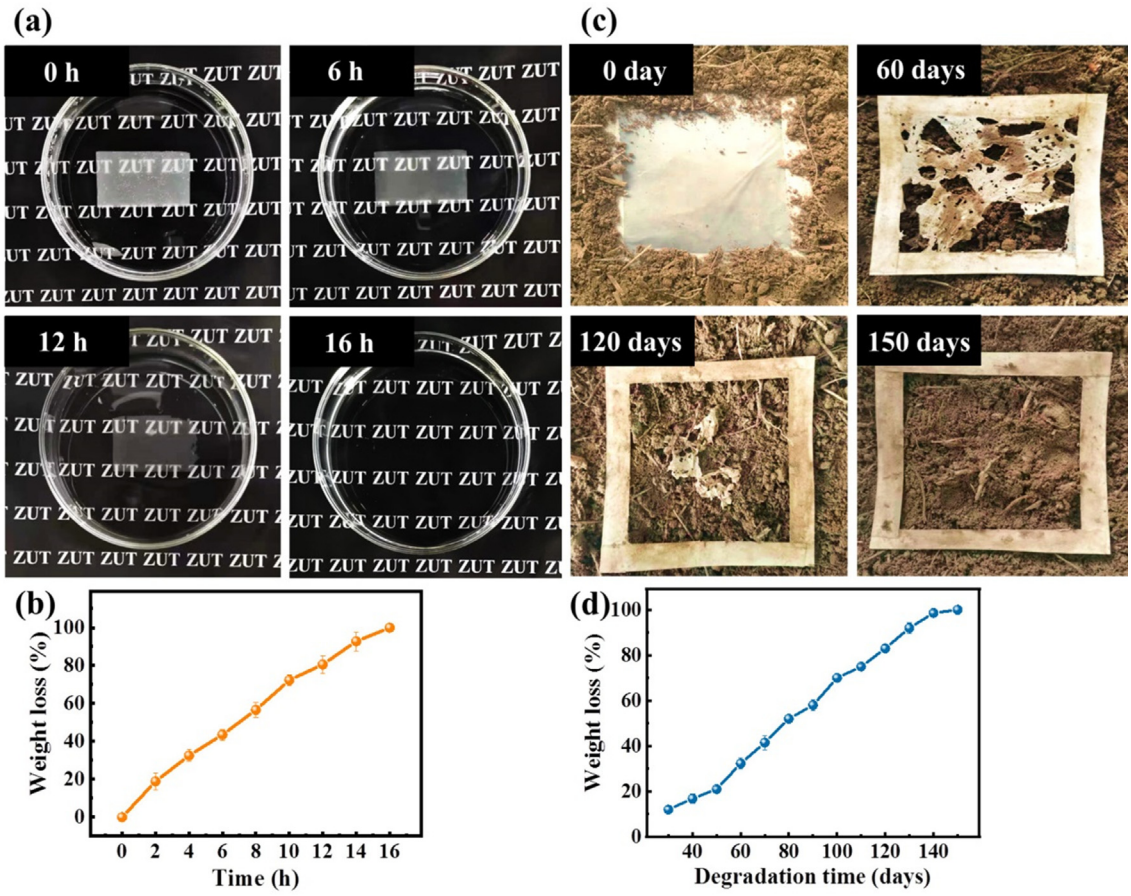

Fig. 5. (a) Time-dependent enzymatic degradation images of the MSM-PLA (3/3, 15 mg) and (b) the corresponding weight loss as a function of time. (c) Images showing the soil burial degradation of the MSM-PLA (3/3, 40 mg) under natural conditions and (d) the corresponding weight loss as a function of time.

with a further increase in the TN-PLA content, despite the improved filtration efficiency, the significant increase in pressure drop brought about the decreased Q_f value from 0.097 Pa^{-1} to 0.082 Pa^{-1}, which is mainly because of the dense stacking of TN-PLA. The increase in the number of solid film-bonded fibers increased the drag force of the MSM-PLA to the airflow (Fig. 4c).

We further evaluated the practical applicability of the 3/3 multi-scale structured membrane by testing the filtration efficiency and pressure drop for NaCl $PM_{0.3}$ under different wind speeds. As shown in Fig. 4d-e, as the airflow rate increased from 32 L min^{-1} to 90 L min^{-1}, the NaCl $PM_{0.3}$ filtration efficiency was almost unchanged and only decreased from 99.996% to 99.967%, while maintaining a high Q_f of 0.026 Pa^{-1}, which indicates the excellent filtration stability of the membrane. This is mainly attributed to the robust interception capacity endowed by the stable multi-scale structure.

3.4. Biodegradability of MSM-PLA

Based on the above analysis, it can be concluded that the obtained MSM-PLA with a spinning unit ratio of 3/3 possesses an excellent integrated performance, and it is more suitable for high-performance mask applications.

More importantly, in comparison to the filter elements of commercial masks or respirators, the obtained MSM-PLA was made entirely of green biodegradable PLA. Its biodegradability was demonstrated through an enzymolysis experiment and outdoor soil burial. As shown in Fig. 5a, with the extension of time, the PLA multiscale structured membrane became thinner, and the lettering below became clearer. After 16 h, the PLA nanofiber membrane was completely decomposed by proteinase K at a temperature of 60 °C (Fig. 5b). The Fig. 5c-d show that after 150 days of outdoor soil burial, the WL of the multi-scale structured membrane was 100%, which could be attributed to the larger

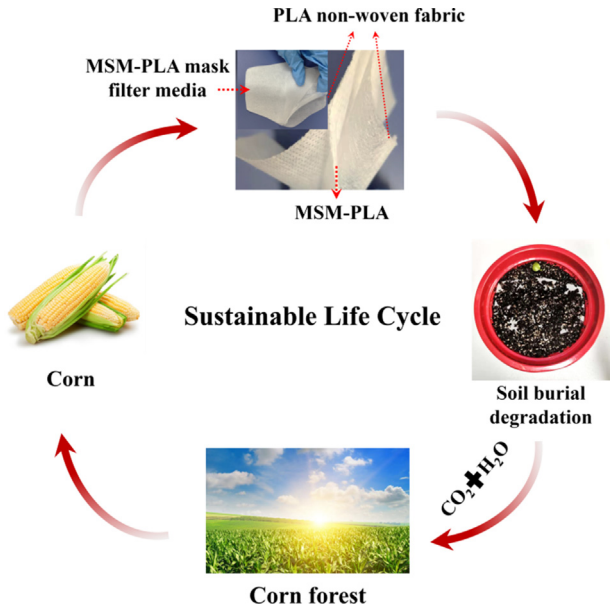

Fig. 6. Sustainable life cycle of MSM-PLA mask filter media.

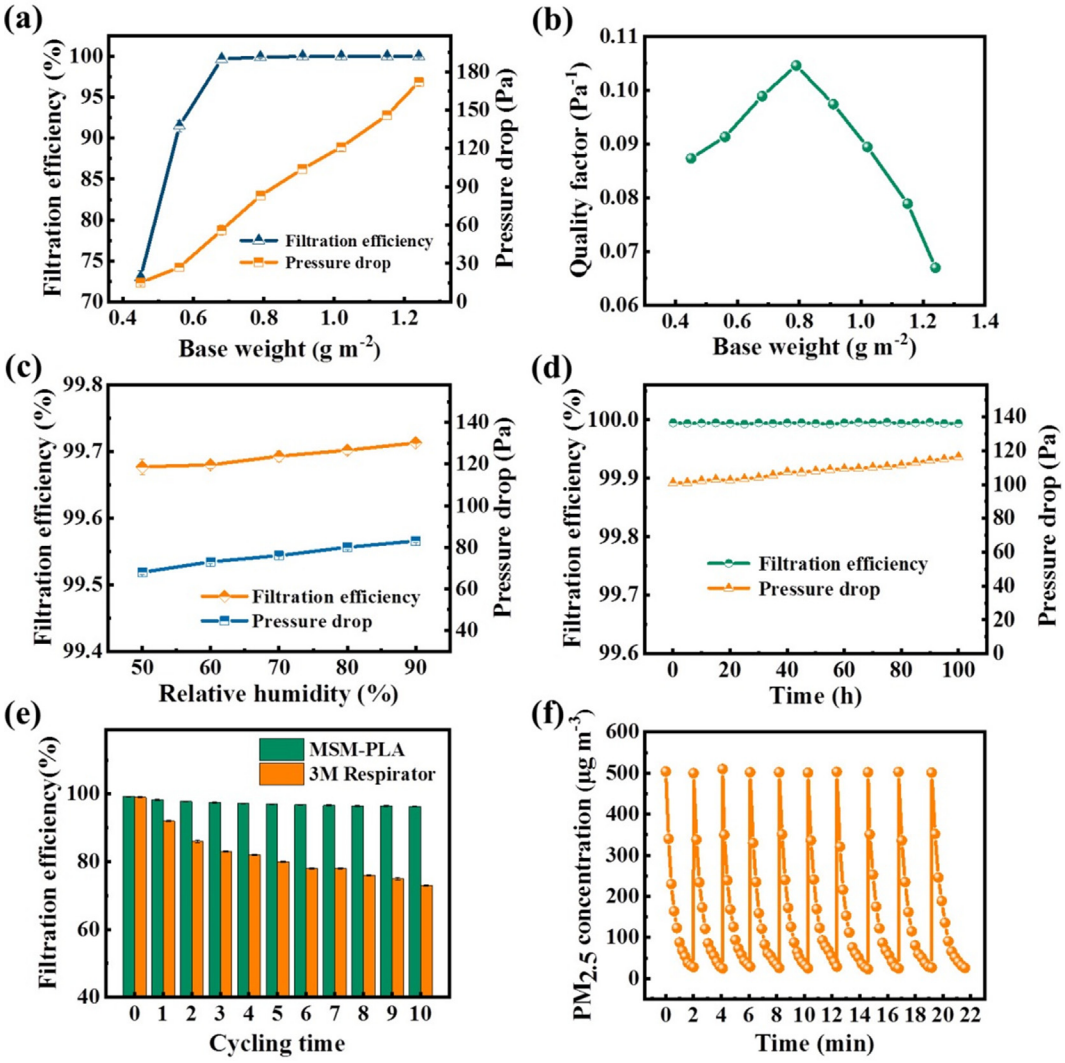

Fig. 7. (a) Filtration performance and (b) quality factor of the MSM-PLA (3/3) with various base weights. (c) Filtration performance of the MSM-PLA (3/3) under different relative humidity and (d) the long-term filtration stability of the MSM-PLA (3/3) under 90% humidity. (e) Filtration efficiency of MSM-PLA mask filter media and 3 M respirator after 10 cycles of soaking in water. (f) Durable PM2.5 removal performance under continuous hazardous level of $PM_{2.5}$ pollution.

interface between water and microorganisms in the soil due to the large surface area of the nanofibers.

Moreover, PLA as a raw material is made from starch extracted from plants, such as corn, wheat, cassava, and so on [33,34]. In addition, through photosynthesis, the CO_2 and H_2O produced by PLA degradation can be utilized by plants, which is a recyclable and sustainable process [45,46] (Fig. 6). Therefore, the use of PLA raw materials is expected to alleviate environmental pollution and resource waste caused by the existing discarded masks, thus paving the way for applying green sustainable masks and is of great significance to the healthy development of the environment.

3.5. Air filtration performance of MSM-PLA mask filter media

As shown in Fig. 6, the three-layer mask filter media was prepared by an ultrasonic composite process, including PLA nonwoven fabric as the inner and outer layers, and multiscale structured membrane as the intermediate layer.

The basis weight of nanofiber membranes is one of the critical factors affecting the filtration efficiency of the mask. MSM-PLA (3/3) with different base weights was obtained by adjusting the receiving speed, denoted as P1-P8. Their filtration performance is presented in Fig. 7a-b. The filtration efficiency of P3 (0.68 g m^{-2}) can easily achieve > 99%. Combined with the true nanoscale diameter and multi-scale structure, a slight increase in the base weight can greatly enhance the removal efficiency, which is attributed to the reduction in pore size. P5 (0.91 g m^{-2}) can remove the NaCl $PM_{0.3}$ with a filtration efficiency of 99.996%, while maintaining a low pressure drop of 104 Pa and the highest quality factor of 0.097 Pa^{-1}. More importantly, at the similar filtration efficiency, the weight of the MSM-PLA is less than one third times that of the existing nanofiber filters and far lower than that of commercial PP melt-blown microfiber mat, which greatly saves resources and improves economic benefits. Furthermore, the comparison of Q_f value from other electrospun nanofiber filters were summarized in Fig. S9. Compared with most of earlier studies, the MSM-PLA exhibited better comprehensive filtration performance [21,29,47–54].

In addition, considering the complexity of the outdoor humid atmosphere, the filtration performance of the filter under different environmental humidities was evaluated (Fig. 7c). Even at an extreme humidity of 90% (higher than the real haze environment) [29], the filters still maintained a high filtration efficiency of > 99.99% after 100 h (Fig. 7d), indicating good environmental

stability. Furthermore, the durable recycling performance of the filter was investigated, which is related to whether people can obtain long-term protection from PM pollution and virus transmission. The filter and 3 M respirator were soaked in water and dried in an oven. The process was repeated 10 times. As shown in Fig. 7e, it can be found that after several cycles, the filtration efficiency of 3 M mask quickly drops to 80%, and finally to 73%, while the efficiency of the filter remained over 95% after 10 cycles. Similarly, to verify the actual use of purification for the PM, we simulated the purification process of the filter under heavy haze conditions ($PM_{2.5}$ concentration of > 500 μg m^{-3}) caused by burning the mosquito killing tablets. Fig. 7f shows that after 10 cycles, one purification cycles from > 500 μg m^{-3} to < 40 μg m^{-3} almost remained unchanged. From the above experiments, it can be proved that the obtained the MSM-PLA mask filter media has an efficient interception performance and durable filtration stability.

4. Conclusion

A true nanoscale PLA nanofiber with an average size of 37 ± 4 nm was successfully fabricated based on an extremely dilute solution with high conductivity via electrospinning technology. A nanofiber membrane with a multiscale structure was designed and optimized to achieve a small pore size (0.73 μm), high porosity (91.72%), and narrow pore size distribution. It also exhibits excellent mechanical and hydrophobic properties. Compared to commercial 3 M masks, the multiscale structured membrane mask filter shows higher filtration efficiency ($PM_{0.3}$–99.996%), which is more breathable (air resistance of 104 Pa) while maintaining a low basis weight (0.91 g m^{-2}). In addition, after exposure to an outdoor humid environment for 100 h, the prepared mask had a robust filtration efficiency (humidity 90%, filtration efficiency > 99.99%). Through the long-term recycling performance test, the filtration efficiency was much higher than that of commercial 3 M masks (multiscale structured mask filter > 95%). More importantly, unlike commercial masks, the resulting filter has biodegradable properties, and the multiscale structured nanofiber membranes completely degrades after 150 days of outdoor soil burial. This study proposes a new method for the preparation of PLA nanofibers, and we believe that this filter would be a great substitute for existing commercial masks in the future.

CRediT authorship contribution statement

Ling Wang: Data curation, Writing – original draft, Formal analysis. **Yanfei Gao:** Methodology, Writing – review & editing, Validation. **Junpeng Xiong:** Investigation, Writing – review & editing, Supervision. **Weili Shao:** Methodology, Resources, Supervision. **Chen Cui:** Validation, Formal analysis. **Ning Sun:** Investigation, Formal analysis. **Yuting Zhang:** Writing – review & editing. **Shuzhen Chang:** Validation. **Pengju Han:** Methodology, Supervision. **Fan Liu:** Methodology, Supervision. **Jianxin He:** Conceptualization.

Declaration of Competing Interest

The authors declare that they have no known competing financial interests or personal relationships that could have appeared to influence the work reported in this paper.

Acknowledgements

This work is supported by National Natural Science Foundation of China (22002193, 51803244 and U2004178), Key Scientific Research Project of Colleges and Universities in Henan Province (20A540002 and 21A540005), Henan Province University Innovation Talents Support Program (2020 HYTP 032), Department of Science and Technology of Henan Province (212102210123 and 212102210041).

Appendix A. Supplementary material

Supplementary data to this article can be found online at https://doi.org/10.1016/j.jcis.2021.08.079.

References

[1] P. Zhou, X.L. Yang, X.G. Wang, B. Hu, L. Zhang, W. Zhang, H.R. Si, Y. Zhu, B. Li, C. L. Huang, H.D. Chen, J. Chen, Y. Luo, H. Guo, R.D. Jiang, M.Q. Liu, Y. Chen, X.R. Shen, X. Wang, X.S. Zheng, K. Zhao, Q.J. Chen, F. Deng, L.L. Liu, B. Yan, F.X. Zhan, Y.Y. Wang, G.F. Xiao, Z.L. Shi, A pneumonia outbreak associated with a new coronavirus of probable bat origin, Nature 579 (7798) (2020) 270–273.
[2] C. Wang, P.W. Horby, F.G. Hayden, G.F. Gao, A novel coronavirus outbreak of global health concern, The Lancet 395 (10223) (2020) 470–473.
[3] J. Howard, A. Huang, Z. Li, Z. Tufekci, V. Zdimal, H.M. van der Westhuizen, A. von Delft, A. Price, L. Fridman, L.H. Tang, V. Tang, G.L. Watson, C.E. Bax, R. Shaikh, F. Questier, D. Hernandez, L.F. Chu, C.M. Ramirez, A.W. Rimoin, An evidence review of face masks against COVID-19, Proc. Natl. Acad. Sci. U.S.A. 118 (4) (2021) e2014564118.
[4] J.C. Prata, A.L.P. Silva, T.R. Walker, A.C. Duarte, T. Rocha-Santos, COVID-19 pandemic repercussions on the use and management of plastics, Environ. Sci. Technol. 54 (13) (2020) 7760–7765.
[5] A.L. Patricio Silva, J.C. Prata, T.R. Walker, A.C. Duarte, W. Ouyang, D. Barcelo, T. Rocha-Santos, Increased plastic pollution due to COVID-19 pandemic: challenges and recommendations, Chem. Eng. J. 405 (2021) 126683.
[6] H. Chowdhury, T. Chowdhury, S.M. Sait, Estimating marine plastic pollution from COVID-19 face masks in coastal regions, Mar. Pollut. Bull. 168 (2021) 7.
[7] C.L. Dybas, Surgical masks on the beach: COVID-19 and marine plastic pollution, Oceanography (Washington D.C.) 34 (1) (2021).
[8] O.O. Fadare, E.D. Okoffo, Covid-19 face masks: a potential source of microplastic fibers in the environment, Sci. Total Environ. 737 (2020) 140279.
[9] A. Ragusa, A. Svelato, C. Santacroce, P. Catalano, V. Notarstefano, O. Carnevali, F. Papa, M.C.A. Rongioletti, F. Baiocco, S. Draghi, E. D'Amore, D. Rinaldo, M. Matta, E. Giorgini, Plasticenta: first evidence of microplastics in human placenta, Environ. Int. 146 (2021) 106274.
[10] T.A. Aragaw, Surgical face masks as a potential source for microplastic pollution in the COVID-19 scenario, Mar. Pollut. Bull. 159 (2020) 111517.
[11] L. Wang, Y. Bian, C.K. Lim, Z. Niu, P.K.H. Lee, C. Chen, L. Zhang, W.A. Daoud, Y. Zi, Tribo-charge enhanced hybrid air filter masks for efficient particulate matter capture with greatly extended service life, Nano Energy 85 (2021) 106015.
[12] S. Choi, H. Jeon, M. Jang, H. Kim, G. Shin, J.M. Koo, M. Lee, H.K. Sung, Y. Eom, H. S. Yang, J. Jegal, J. Park, D.X. Oh, S.Y. Hwang, Biodegradable, efficient, and breathable multi-use face mask filter, Adv. Sci. 8 (6) (2021) 2003155.
[13] S. Li, D.R. Chen, F. Zhou, S.C. Chen, Effects of relative humidity and particle hygroscopicity on the initial efficiency and aging characteristics of electret HVAC filter media, Build. Environ. 171 (2020) 106669.
[14] R. Thakur, D. Das, A. Das, Electret air filters, Sep. Purif. Rev. 42 (2) (2013) 87–129.
[15] H. Liu, L. Liu, J. Yu, X. Yin, B. Ding, High-efficiency and super-breathable air filters based on biomimetic ultrathin nanofiber networks, Compos. Commun. 22 (2020) 100493.
[16] Kenry, C.T. Lim, Lim, Nanofiber technology: current status and emerging developments, Prog. Polym. Sci. 70 (2017) 1–17.
[17] J. Xue, J. Xie, W. Liu, Y. Xia, Electrospun nanofibers: new concepts, materials, and applications, Acc. Chem. Res. 50 (8) (2017) 1976–1987.
[18] G. Gong, C. Zhou, J. Wu, J. Xu, L.J.A.N. Jiang, Nanofibrous adhesion: the twin of gecko adhesion, ACS Nano 9 (4) (2015) 3721–3727.
[19] V. Thavasi, G. Singh, S. Ramakrishna, Electrospun nanofibers in energy and environmental applications, Energy Environ. Sci. 1 (2) (2008) 205–221.
[20] M. Zhu, J. Han, F. Wang, W. Shao, R. Xiong, Q. Zhang, H. Pan, Y. Yang, S.K. Samal, F. Zhang, C. Huang, Electrospun nanofibers membranes for effective air filtration, Macromol. Mater. Eng. 302 (1) (2017) 16300353.
[21] B. Liu, S. Zhang, X. Wang, J. Yu, B. Ding, Efficient and reusable polyamide-56 nanofiber/nets membrane with bimodal structures for air filtration, J. Colloid Interface Sci. 457 (2015) 203–211.
[22] X. Li, N.a. Wang, G. Fan, J. Yu, J. Gao, G. Sun, B. Ding, Electreted polyetherimide-silica fibrous membranes for enhanced filtration of fine particles, J. Colloid Interface Sci. 439 (2015) 12–20.
[23] F. Liu, M. Li, W. Shao, W. Yue, B. Hu, K. Weng, Y. Chen, X.i. Liao, J. He, Preparation of a polyurethane electret nanofiber membrane and its air-filtration performance, J. Colloid Interface Sci. 557 (2019) 318–327.
[24] S. Zhang, H. Liu, N. Tang, J. Ge, J. Yu, B. Ding, Direct electronetting of high-performance membranes based on self-assembled 2D nanoarchitectured networks, Nat. Commun. 11 (1) (2020) 1040.
[25] X. Wang, B. Ding, G. Sun, M. Wang, J. Yu, Electro-spinning/netting: a strategy for the fabrication of three-dimensional polymer nano-fiber/nets, Prog. Mater. Sci. 58 (8) (2013) 1173–1243.

[26] S. Zhang, H. Liu, N. Tang, N. Ali, J. Yu, B. Ding, Highly efficient, transparent, and multifunctional air filters using self-assembled 2D nanoarchitectured fibrous networks, ACS Nano 13 (11) (2019) 13501–13512.
[27] S. Zhang, H. Liu, X. Yin, Z. Li, J. Yu, B. Ding, Tailoring mechanically robust poly (m-phenylene isophthalamide) nanofiber/nets for ultrathin high-efficiency air filter, Sci. Rep. 7 (2017) 40550.
[28] F. Zuo, S. Zhang, H. Liu, H. Fong, X. Yin, J. Yu, B. Ding, Free-standing polyurethane nanofiber/nets air filters for effective PM capture, Small 13 (46) (2017) 1702139.
[29] H. Liu, S. Zhang, L. Liu, J. Yu, B. Ding, A fluffy dual-network structured nanofiber/net filter enables high-efficiency air filtration, Adv. Funct. Mater. 29 (39) (2019) 1904108.
[30] W.K. Essa, S.A. Yasin, I.A. Saeed, G.A.M. Ali, Nanofiber-based face masks and respirators as COVID-19 protection: a review, Membr. 11 (4) (2021) 250.
[31] H. Souzandeh, Y. Wang, A.N. Netravali, W.H. Zhong, Towards sustainable and multifunctional air-filters: a review on biopolymer-based filtration materials, Polym. Rev. 59 (4) (2019) 651–686.
[32] V. Shanmugam, K. Babu, T.F. Garrison, A.J. Capezza, R.T. Olsson, S. Ramakrishna, M.S. Hedenqvist, S. Singha, M. Bartoli, M. Giorcelli, G. Sas, M. Forsth, O. Das, A. Restas, F. Berto, Potential natural polymer-based nanofibers for the development of facemasks in countering viral outbreaks, J. Appl. Polym. Sci. 138 (27) (2021) 50658.
[33] M.A. Elsawy, K.-H. Kim, J.-W. Park, A. Deep, Hydrolytic degradation of polylactic acid (PLA) and its composites, Renew. Sust. Energ. Rev. 79 (2017) 1346–1352.
[34] K. Hamad, M. Kaseem, M. Ayyoob, J. Joo, F. Deri, Polylactic acid blends: the future of green, light and tough, Prog. Polym. Sci. 85 (2018) 83–127.
[35] Z.C. Xiong, R.L. Yang, Y.J. Zhu, F.F. Chen, L.Y. Dong, Flexible hydroxyapatite ultralong nanowire-based paper for highly efficient and multifunctional air filtration, J. Mater. Chem. A 5 (33) (2017) 17482–17491.
[36] J. Cui, T. Lu, F. Li, Y. Wang, J. Lei, W. Ma, Y. Zou, C. Huang, Flexible and transparent composite nanofibre membrane that was fabricated via a "green" electrospinning method for efficient particulate matter 2.5 capture, J. Colloid Interface Sci. 582 (2021) 506–514.
[37] J. Cui, Y. Wang, T. Lu, K. Liu, C. Huang, High performance, environmentally friendly and sustainable nanofiber membrane filter for removal of particulate matter 1.0, J. Colloid Interface Sci. 597 (2021) 48–55.
[38] H. Wan, N.a. Wang, J. Yang, Y. Si, K. Chen, B. Ding, G. Sun, M. El-Newehy, S.S. Al-Deyab, J. Yu, Hierarchically structured polysulfone/titania fibrous membranes with enhanced air filtration performance, J. Colloid Interface Sci. 417 (2014) 18–26.
[39] T. Ahmed, M. Shahid, F. Azeem, I. Rasul, A.A. Shah, M. Noman, A. Hameed, N. Manzoor, I. Manzoor, S. Muhammad, Biodegradation of plastics: current scenario and future prospects for environmental safety, Environ. Sci. Pollut. Res. Int. 25 (8) (2018) 7287–7298.
[40] S.M. Emadian, T.T. Onay, B. Demirel, Biodegradation of bioplastics in natural environments, Waste Manag. 59 (2017) 526–536.
[41] A. Folino, A. Karageorgiou, P.S. Calabrò, D. Komilis, Biodegradation of wasted bioplastics in natural and industrial environments: a review, Sustainability 12 (15) (2020) 6030.
[42] H. Liu, S. Zhang, L. Liu, J. Yu, B. Ding, High-performance $PM_{0.3}$ air filters using self-polarized electret nanofiber/nets, Adv. Funct. Mater. 30 (13) (2020) 1909554.
[43] A. Amin, A.A. Merati, S.H. Bahrami, R. Bagherzadeh, Effects of porosity gradient of multilayered electrospun nanofibre mats on air filtration efficiency, J. Textile Inst. 108 (9) (2016) 1563–1571.
[44] X. Zhao, S. Wang, X. Yin, J. Yu, B. Ding, Slip-effect functional air filter for efficient purification of $PM_{2.5}$, Sci. Rep. 6 (2016) 35472.
[45] O. Faruk, A.K. Bledzki, H.-P. Fink, M. Sain, Biocomposites reinforced with natural fibers: 2000–2010, Prog. Polym. Sci. 37 (11) (2012) 1552–1596.
[46] E. Castro-Aguirre, F. Iñiguez-Franco, H. Samsudin, X. Fang, R. Auras, Poly(lactic acid)-mass production, processing, industrial applications, and end of life, Adv. Drug Deliv. Rev. 107 (2016) 333–366.
[47] Y. Xiao, Y. Wang, W. Zhu, J. Yao, C. Sun, J. Militky, M. Venkataraman, G. Zhu, Development of tree-like nanofibrous air filter with durable antibacterial property, Sep. Purif. Technol. 259 (2021) 118135.
[48] Z. Wang, Z. Pan, J. Wang, R. Zhao, A novel hierarchical structured poly(lactic acid)/titania fibrous membrane with excellent antibacterial activity and air ailtration performance, J. Nanomater. 2016 (2016) 1–17.
[49] K. Zhang, Z. Li, W. Kang, N. Deng, J. Yan, J. Ju, Y. Liu, B. Cheng, Preparation and characterization of tree-like cellulose nanofiber membranes via the electrospinning method, Carbohydr. Polym. 183 (2018) 62–69.
[50] H. Li, Z. Wang, H. Zhang, Z. Pan, Nanoporous PLA/(chitosan nanoparticle) composite fibrous membranes with excellent air filtration and antibacterial performance, Polymers (Basel) 10 (10) (2018) 1085.
[51] Z. Wang, C. Zhao, Z. Pan, Porous bead-on-string poly(lactic acid) fibrous membranes for air filtration, J. Colloid Interface Sci. 441 (2015) 121–129.
[52] X. Chen, Y. Xu, M. Liang, Q. Ke, Y. Fang, H.e. Xu, X. Jin, C. Huang, Honeycomb-like polysulphone/polyurethane nanofiber filter for the removal of organic/inorganic species from air streams, J. Hazard. Mater. 347 (2018) 325–333.
[53] Z. Shao, J. Jiang, X. Wang, W. Li, L. Fang, G. Zheng, Self-Powered Electrospun Composite Nanofiber Membrane for Highly Efficient Air Filtration, Nanomaterials (Basel) 10 (9) (2020).
[54] Z. Li, W. Kang, H. Zhao, M. Hu, J. Ju, N. Deng, B. Cheng, Fabrication of a polyvinylidene fluoride tree-like nanofiber web for ultra high performance air filtration, RSC Adv. 6 (94) (2016) 91243–91249.